Characterization of HAZ of API X70 Microalloyed Steel Welded by Cold-wire Tandem Submerged Arc Welding

MOHSEN MOHAMMADIJOO[1], STEPHEN KENNY[1,2], LAURIE COLLINS[2], HANI HENEIN[1], and DOUGLAS G. IVEY[1,*]

[1]Department of Chemical and Materials Engineering, University of Alberta, Edmonton, AB, Canada T6G 1H9

[2]R&D Division, Evraz Inc. NA, P.O. Box 1670, Regina, SK, Canada S4P 3C7

[*]Corresponding author. Prof., Ph.D.; Tel.: +1 780 4922957; Fax: +1 780 4922881

E-mail address: divey@ualberta.ca (D.G. IVEY)

ABSTRACT

High strength low carbon microalloyed steels may be adversely affected by the high heat input and thermal cycle that they experience during tandem submerged arc welding (TSAW). The heat affected zone (HAZ), particularly the coarse grained heat affected zone (CGHAZ), i.e., the region adjacent to the fusion line, has been known to show lower fracture toughness compared with the rest of the steel. The deterioration in toughness of the CGHAZ is attributed to the formation of martensite-austenite (M-A) constituents, local brittle zones (LBZ) and large prior austenite grains (PAG). In the present work, the influence of the addition of a cold wire at various wire feed rates in cold-wire tandem submerged arc welding (CWTSAW), a recently developed welding process for pipeline manufacturing, on the microstructure and mechanical properties of the HAZ of a microalloyed steel has been studied. The cold wire moderates the heat input of welding by consuming the heat of the trail electrode. Macrostructural analysis showed a decrease in the CGHAZ size by addition of a cold wire. Microstructural evaluation, using both tint etching optical microscopy (TEOM) and scanning electron microscopy (SEM), indicated the formation of finer PAGs and less fraction of M-A constituents with refined morphology within the CGHAZ when the cold wire was fed at 25.4 cm/min. This resulted in an improvement in the HAZ impact fracture toughness. These improvements are attributed to lower actual heat introduced to the weldment and lower peak temperature in the CGHAZ by cold wire addition. However, a faster feed rate of the cold wire at 76.2 cm/min adversely affected the toughness due to the formation of slender M-A constituents caused by the relatively faster cooling rate in the CGHAZ.

Keywords: Martensite-austenite constituent, Toughness, Microhardness, Welding process, Microalloyed steel.

I. INTRODUCTION

Tandem submerged arc welding (TSAW), i.e., submerged arc welding with two to five electrodes [1–3], has been extensively utilized to fabricate high strength low alloy steel pipelines, pressure vessels, structures and wind turbine towers [4,5]. TSAW offers several advantages over other welding processes, such as high deposition rate, deep penetration, high quality welds and the ability to weld thick plates due to its high heat input [6,7]. The fracture toughness of the heat affected zone (HAZ), particularly the coarse grained heat affected zone (CGHAZ), of microalloyed steel welds tends to weaken due to the high heat input and thermal cycles that the steel experiences during welding. The reduction in toughness in the CGHAZ is attributed to the formation of large prior austenite grains (PAGs) and martensite-austenite (M-A) constituents, which are characterized as localized brittle zones (LBZ), as a result of the high peak temperature and relatively fast cooling rate in the CGHAZ [8–12]. Davis et al. [13,14] and Reichert et al. [15] found that the formation of a network of enlarged M-A constituents along the PAG boundaries resulted in cleavage crack initiation in the HAZ. Moeinifar et al. [16] suggested that a reduced fraction of M-A constituents in the CGHAZ was beneficial to the impact toughness. However, the fraction and size of M-A constituents are essentially dependent on the PAG size. Yu et al. [10] and Li et al. [11] showed that the fraction and shape of M-A constituents were increased by coarsening the PAG size in the CGHAZ. They found that a coarse PAG size, associated with coarse M-A constituents, is the dominant factor in promoting brittle fracture in the CGHAZ. Gharibshahiyan et al. [17] reported that the formation of coarser PAGs in the CGHAZ has a detrimental effect on the toughness of the HAZ. Yang and Bhadeshia [18] and Garcia-Junceda et al. [19] showed that the martensite start temperature (Ms) increases with an increase in the PAG size, which results in a higher volume fraction of martensite.

In the present work, cold-wire TSAW (CWTSAW) is developed to improve the microstructure and the mechanical properties of the HAZ of a X70 microalloyed steel weld, while retaining appropriate weld geometry. The additional cold wire fed into the tandem weld pool essentially increases the deposition rate, resulting in better welding productivity for the welding process without increasing the heat input compared with the TSAW process [20–22]. In our previous studies [23,24] the CWTSAW process parameters were correlated with the dilution, geometry characteristics and microhardness properties of the weld metal (WM) and HAZ. Incorporating a cold wire in TSAW moderates the heat input through transfer of some of the excess energy of the trail electrode, which lowers the amount of heat introduced to the weldment [20–22]. Accordingly, better quality welds were achieved at lower heat inputs per mass of deposited material and with a substantial reduction in arcing time leading to the formation of a smaller and shorter weld pool (compared with TSAW without a cold wire) [23,24]. As such, CWTSAW technology is a promising technique for pipe seam welds commonly used in the pipeline industry. The present study characterizes the macrostructure, mechanical properties and microstructure alterations in the HAZ of a typical microalloyed steel and their evolution by varying the cold wire feeding rate in the CWTSAW process. Microstructural characterization is carried out using tint etching optical microscopy (TEOM) and scanning electron microscopy (SEM). Charpy V-notch impact testing and microhardness testing are performed to investigate and correlate the properties changes with microstructure alterations in the HAZ of samples prepared by CWTSAW. The geometry characteristics are analyzed using stereomicroscopy.

II. MATERIALS AND EXPERIMENTAL PROCEDURE

A. *Materials and Welding Process*

API X70 microalloyed steel plates with a thickness of 13.4±0.3 mm, produced by Evraz Inc. NA through thermo-mechanical controlled processing (TMCP) [25], were V-shape beveled with an angle and depth of 80º±5° and 4 mm, respectively, prior to welding. Six welding runs at three different cold wire feed rates were carried out to prepare the weld samples. The weld samples were prepared using two 4 mm diameter EA2 electrodes (according to AWS-A5.23/ASME-SFA5.23) and one cold wire with the same diameter and composition as the electrodes. BF6.5 flux was chosen according to EN 760 (Bavaria, Germany). The chemical compositions of the microalloyed steel and consumable electrodes are given in Table I. According to Easterling [26], the welding crack susceptibility of steels is usually expressed in terms of a carbon equivalent that shows composition allowances to avoid cold cracking or hydrogen cracking. For low carbon microalloyed steels, the welding crack susceptibility index, Pcm, is calculated according to the Ito-Bessyo equation [27].

$$\boldsymbol{P_{cm}} = \%C + \frac{\%Si}{30} + \frac{\%Mn + \%Cu + \%Cr}{20} + \frac{\%Mo}{15} + \frac{\%V}{10} + \frac{\%Ni}{60} + 5\%B \qquad [1]$$

The lead and trail electrodes were operated using direct current electrode positive (DCEP) and square wave alternating current (ACSQ) polarity, respectively, with constant current type power sources. The influence of CWTSAW process parameters on the geometry, dilution and microhardness of the weld and the HAZ was investigated and optimized in a previous work of the authors [23,24]. The present CWTSAW process setup has been developed based on the optimized welding parameters. The welding conditions to fabricate the microalloyed steel joint are presented in Table II. The steel plate geometry and the CWTSAW process setup employed to fabricate the weld samples are depicted in Figure 1. The heat input of the welding processes was calculated according to equation 2 [28] and set at 22.2 kJ/cm.

$$HI\left(\frac{kJ}{cm}\right) = \frac{60 \cdot \mu}{1000 \cdot S} \cdot [(V \cdot I)_{Lead} + (V \cdot I)_{Trail}] \qquad [2]$$

where μ is the arc efficiency, which depends on the welding process, and *HI*, *V*, *I* and *TS* are the heat input, voltage, current and travel speed (cm/s), respectively. The arc efficiency for submerged arc welding is 0.9-1.0.

The weld samples were prepared by CWTSAW at cold wire feed rates of 25.4 cm/min and 76.2 cm/min and by TSAW (no cold wire), which are henceforth referred to as CW1, CW3 and TS, respectively. All welding parameters were the same for the processes other than the additional cold wire.

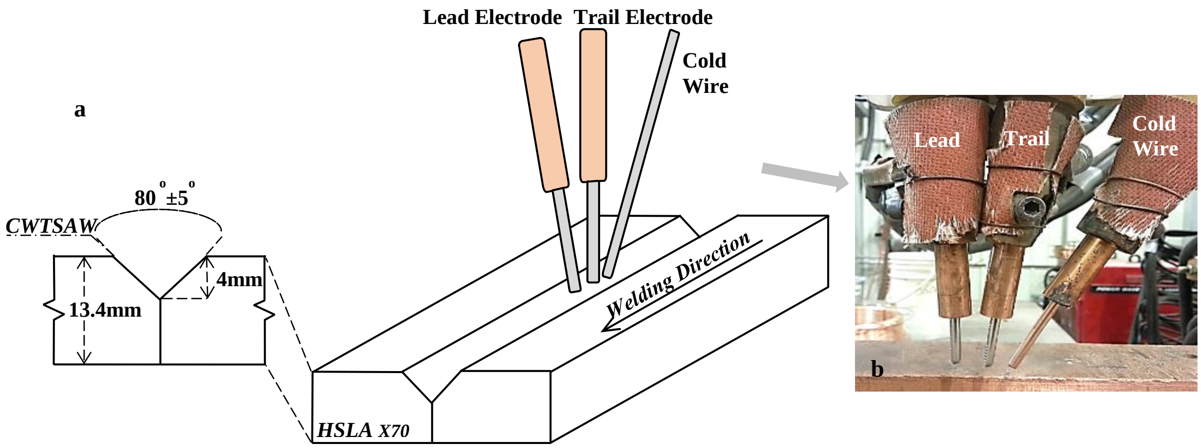

Fig. 1- CWTSAW process setup. (a) Schematic view of joint configuration along with the positioning of the electrodes and cold wire and (b) welding setup designed at Evraz Inc. NA.

B. *Microstructure and Mechanical Testing*

Due to the bulbous shape of the weld metal and the HAZ and the relatively small size of the HAZ, it was not possible to fabricate full size Charpy specimens of the HAZ. As such, subsize Charpy V-notch (CVN) specimens (5 mm x 10 mm x 55 mm) were machined along the transverse welding direction according to ASTM E23-12c [29]. These were extracted as close to the top metal surface as possible to ensure that half of the notch was located in the CGHAZ and half was located in the fine grained heat affected zone (FGHAZ). In order to position the V notch in the HAZ, the specimens were firstly macro-etched with 5% Nital to outline the HAZ boundaries. The Charpy impact tests were then performed at room temperature (RT), 243 K (-30°C) and 228 K (-45°C) and at least five specimens per weld condition and temperature were tested. Figure 2(a) illustrates the location of the notch for the toughness investigation. To analyze the microhardness variation along the weld samples (ASTM E384 [30]), two transverse samples from each weld were extracted according to ASTM E3-11 [31] to increase the number of data sets. A 500 g load was applied for a dwell time of 14 s per indentation using a Wilson-VH3300 microhardness machine (Buehler, Germany). In total, forty test points were examined per weld, with an average of 14-18 indents across each of the FGHAZ and CGHAZ. Figure 2(b) depicts the hardness measurement mapping along a weld sample fabricated using CWTSAW.

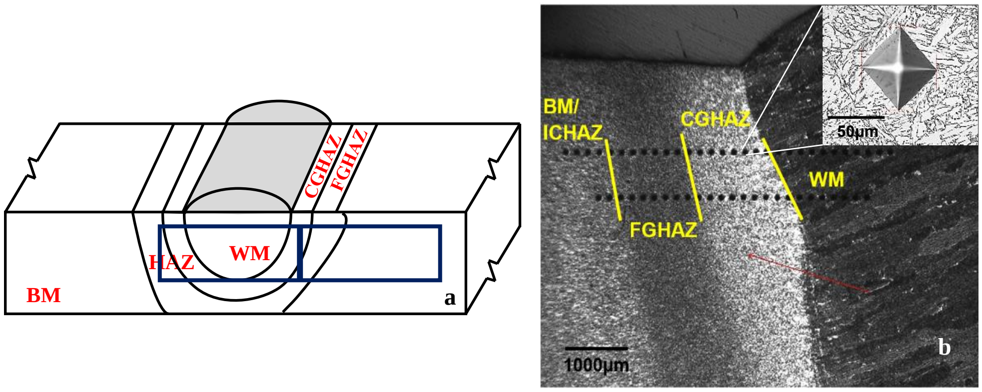

Fig. 2- (a) Schematic view of the CVN specimen extraction from the weld sample. (b) Microhardness mapping along the BM, HAZ and WM of a typical weld prepared by CWTSAW. The micrograph in the inset shows an indentation in the CGHAZ.

Optical microscopy (Olympus BX61) and scanning electron microscopy (Tescan Vega-3 SEM) were utilized to analyze the microstructural changes along the HAZ. The formation and fraction of M-A constituents is dependent on the cooling rate and the PAG size [11,12,32]. Revealing PAG boundaries and M-A constituents in microalloyed steels and their relevant welds can be difficult to achieve and depends very much on the etchant type and time. As such, several etching procedures, using various etchants with different solution concentrations and etching times, were employed. After the etching trials, a chemical solution containing 4 g of picric acid in 96 ml ethanol along with a few drops of HCl acid was selected to reveal the PAG boundaries. The PAG size was analyzed using the mean linear intercept method according to ASTM E112 [33]. Freshly polished weld specimens were then tint etched through a separate process using modified LePera's etchant [34,35] for 30-50 s to reveal different microstructural features. Microstructural analysis indicated a high sensitivity for phase identification to etchant composition and etching time. Quantitative analysis of the M-A constituent was done using ImageJ commercial image analysis software. The fraction of other microstructure features was examined according to ASTM E562 [36]. Fracture analysis of the CVN specimens was carried out by SEM.

III. RESULTS

A. *Charpy Impact Toughness*

The average of the Charpy results and the minimum impact energy for each weld are presented in Figure 3. The minimum Charpy absorbed energy represents the lowest toughness that was measured and may be important from a practical perspective. According to Figure 3, the impact energy (both the average and minimum values) increased at the different testing temperatures when the cold wire was fed at 25.4 cm/min compared with the conventional TSAW process. However, the Charpy results showed no improvement when the cold wire was fed at 76.2 cm/min. Given the fact that fracture toughness of microalloyed steels is influenced by a number of microstructural factors, such as grain size, matrix microstructural features and the shape, size, distribution and fraction of M-A constituents, the microstructure of the HAZ is evaluated and discussed in detail below. The microstructural changes in the HAZ, as a result of cold wire addition, are attributed to changes in the actual heat introduced to the weldment and the cooling rate in the CGHAZ, when cold wire is added to the TSAW process. The large error bars for the HAZ weld samples at 243 K (-30°C) are most likely related to the ductile-to-brittle transition temperature (DBTT) for this steel, which is close to 243 K (-30°C). This interpretation in consistent with Graham [37] who reported that the Charpy absorbed energy data for ferritic steels commonly exhibits large scatter in the DBTT region. However, the results show a consistent trend in CVN impact energy by cold wire addition at different testing temperatures.

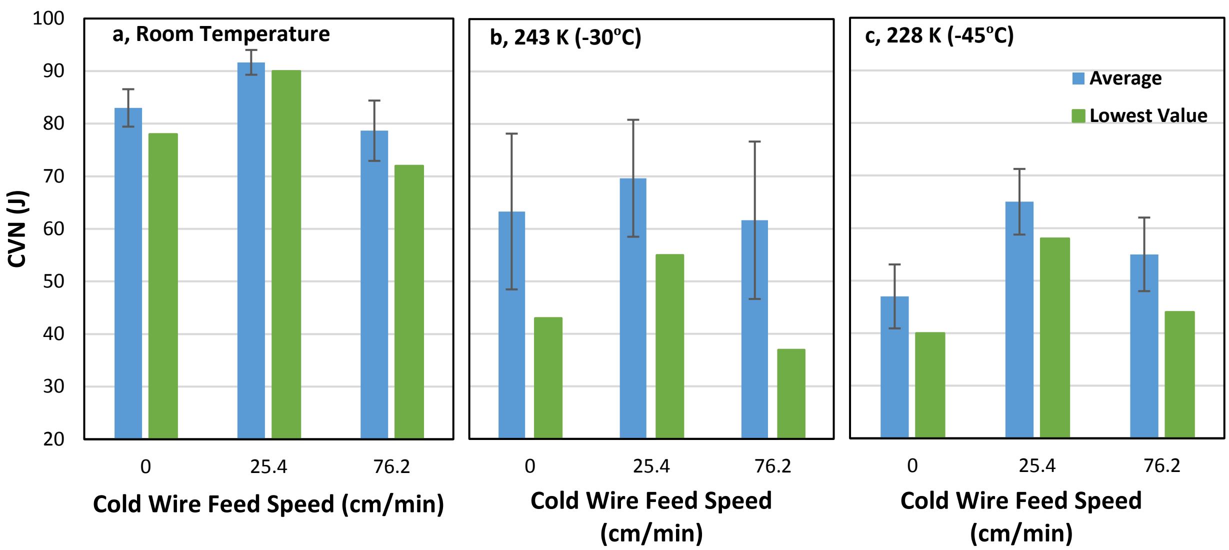

Fig. 3- Charpy impact toughness of the HAZ for steel samples welded by TSAW (no cold wire) and CWTSAW (cold wire addition at 25.4 cm/min and 76.2 cm/min). (a), (b) and (c) represent Charpy results at room temperature (RT), 243 K (-30ºC) and 228 K (-45ºC), respectively.

B. *Microhardness and Macrostructure*

In addition to CVN testing, weld samples fabricated using the CWTSAW and TSAW processes were evaluated in terms of HAZ geometry and microhardness. The resultant CGHAZ area for the CWTSAW process was narrower than that for the TSAW process, due to lower actual heat introduced to the weldment by cold wire addition and the corresponding faster cooling rate. The reduction in the CGHAZ size was larger for the CW3 sample due to the higher cold wire feeding rate of 76.2 cm/min. Macrographs of three weld samples prepared via the CWTSAW and TSAW processes are shown in Figure 4. The results of four geometry measurements indicated a reduction in the CGHAZ area from 21.56±0.63 mm^2 for the TS weld to 20.30±0.50 mm^2 and 17.40±0.63 mm^2 for the CW1 and CW3 welds, respectively. The weld deposition rate was increased by 6% and 17% relative to the TSAW process, when the cold wire was fed at a rate of 25.4 cm/min (10 in/min) and 76.2 cm/min (30 in/min), respectively.

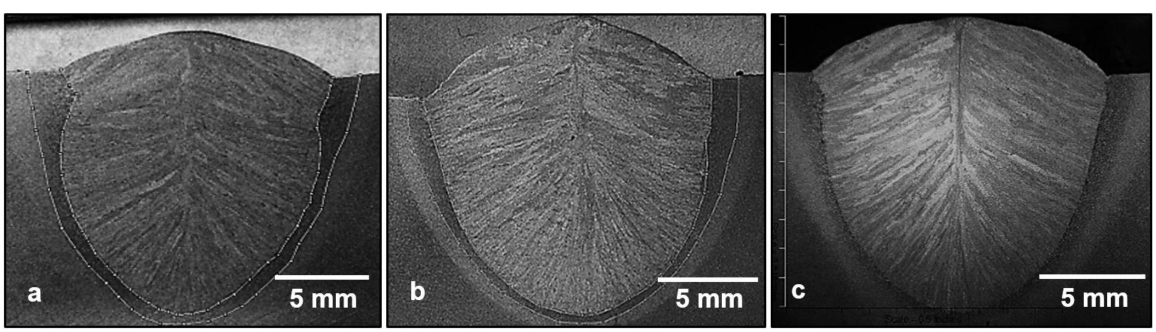

Fig. 4- Macrographs of welded samples: (a) TS, (b) CW1 and (c) CW3.

Microhardness variations along the HAZ and the WM are depicted in Figure 5. The microhardness values of the as-received base metal (BM) was measured as 228±4 HV. As shown in Figure 5, the microhardness of the CGHAZ was reduced by the addition of a cold wire at 25.4 cm/min relative to the TSAW process. However, the average microhardness in the CGHAZ increased when the cold wire was fed at 76.2 cm/min. The different effects of cold wire addition on both microhardness and Charpy impact energy results is attributed to microstructural modifications taking place in the HAZ, due to changes in the actual welding heat input and consequent cooling rate, which are discussed later in this paper. The variation in the fraction, size, distribution and shape of M-A constituents (LBZ) formed within the HAZ of microalloyed steel welds plays a significant role in the variation in mechanical properties in the HAZ, particularly the CGHAZ, which has also been confirmed by Bhadeshia [38,39].

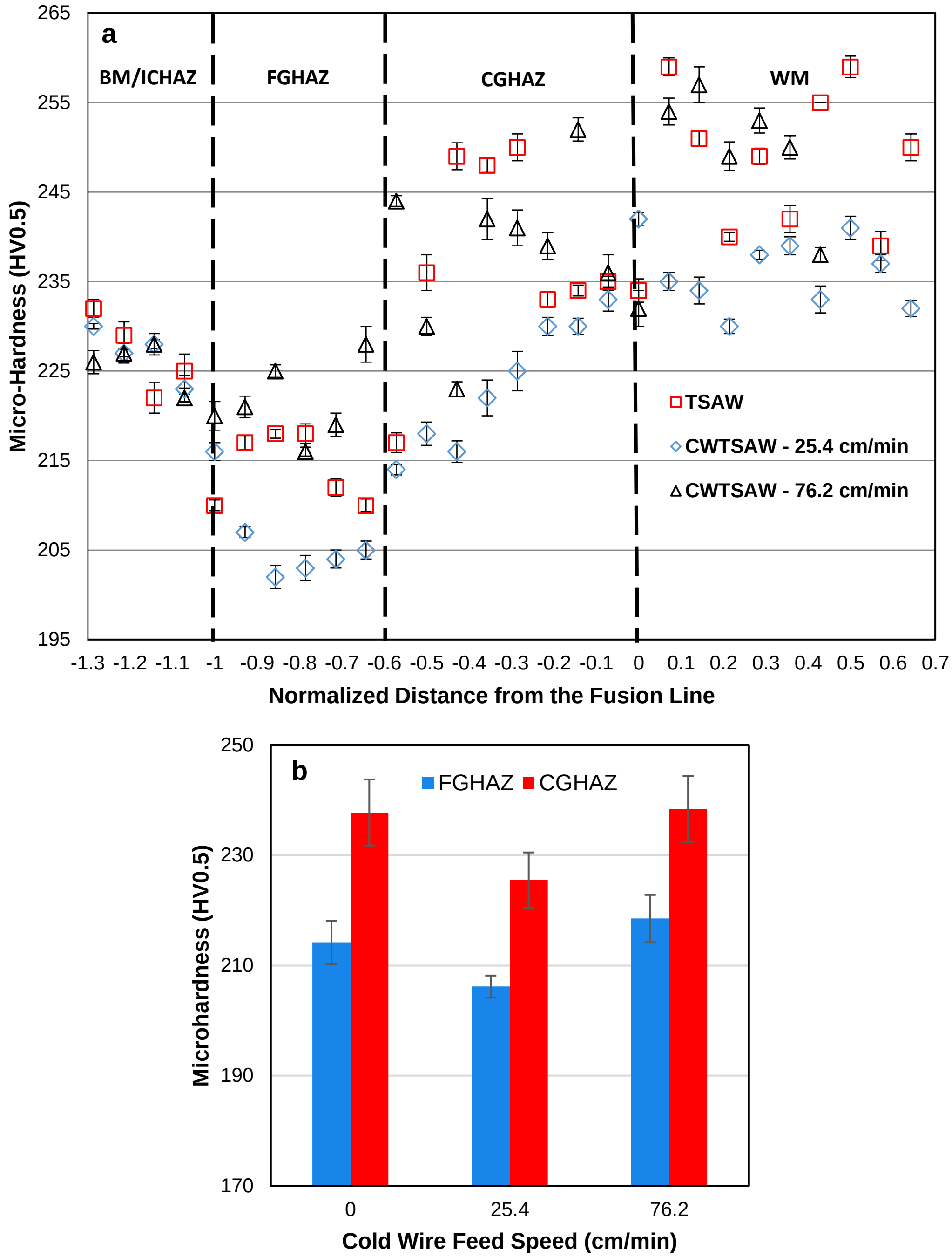

Fig. 5- (a) Microhardness variation within the weld samples. (b) Average microhardness, with standard deviation, for the FGHAZ and CGHAZ of steel samples welded by CWTSAW (cold wire addition at 25.4 cm/min and 76.2 cm/min) and TSAW (no cold wire).

C. *Microstructure*

The microstructure of the X70 microalloyed steel consists of 87% polygonal ferrite, 9% granular bainite, 3% bainitic ferrite and a fine distribution of 1% M-A constituents with a PAG size of ~8 µm. The type and fraction of microstructural features along with the PAG formed in the region adjacent to the weld metal, i.e., the HAZ, are altered due to the heat input and thermal cycles during welding. The PAG size in the CGHAZ (Figure 6(a)-(c)) and the FGHAZ decreased with the addition of the cold wire. The average PAG size in the CGHAZ (0-300 µm away from the fusion line) and FGHAZ (0-200 µm away from the CGHAZ/FGHAZ boundary) for the TS, CW1 and CW3 weld samples are shown in Figure 7(a). The reduction in the PAG size in the CGHAZ is attributed to a reduction in the actual heat introduced to the weldment, a reduction in the retention time in the austenite temperature range, i.e., 1373-1673K (1100-1400ºC), and an increase in the cooling rate by adding the cold wire. The M-A constituent, along with other microstructural features in the CGHAZ and FGHAZ of the three weld samples, are shown in Figure 6(d)-(i). The M-A constituents are revealed as white regions using modified LePera's etchant [34,35]. The amount of the microconstituents is shown in Figure 7(b). SEM secondary electron (SE) micrographs of the CGHAZ of the weld samples are depicted in Figure 8(a)-(c).

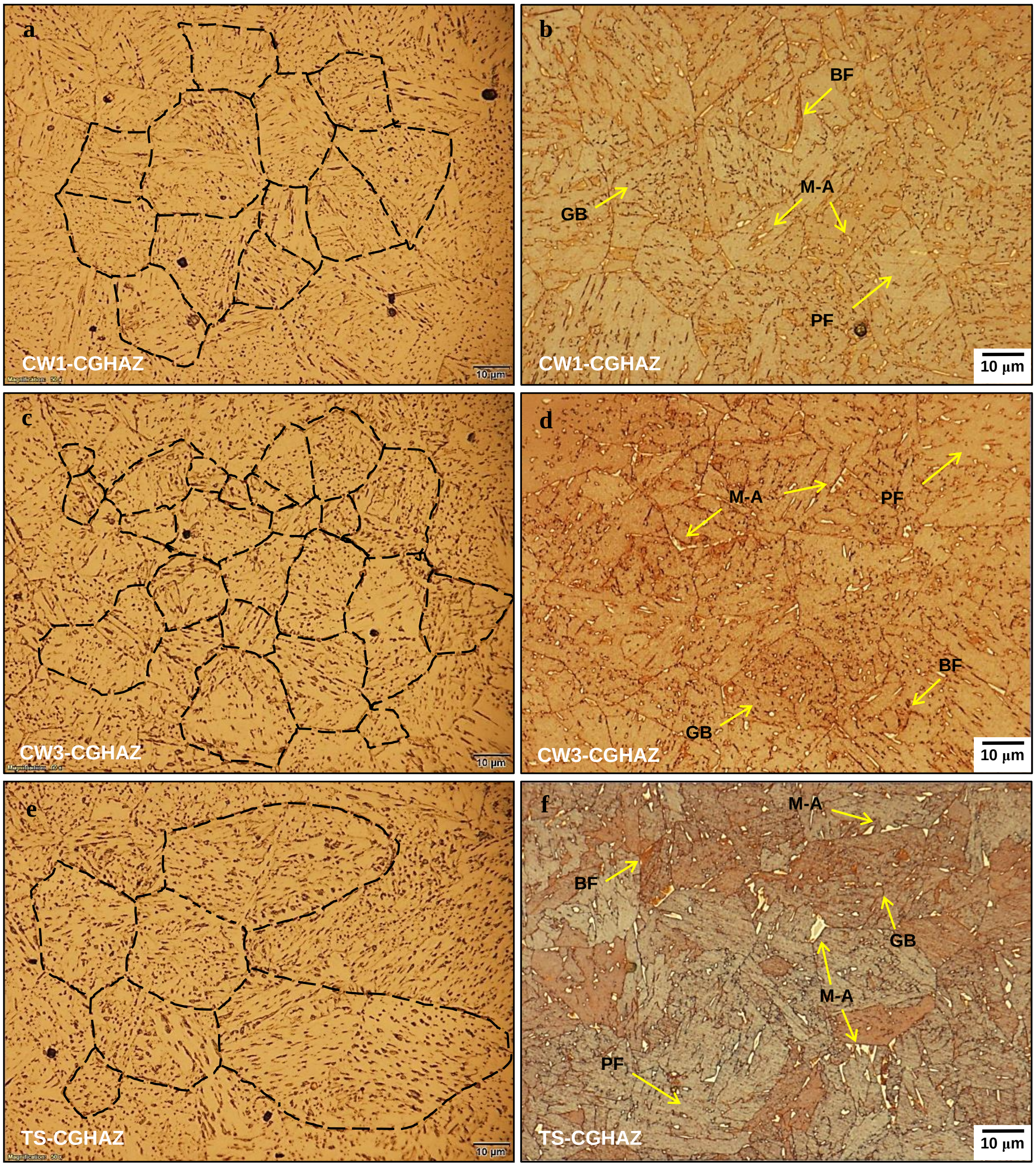

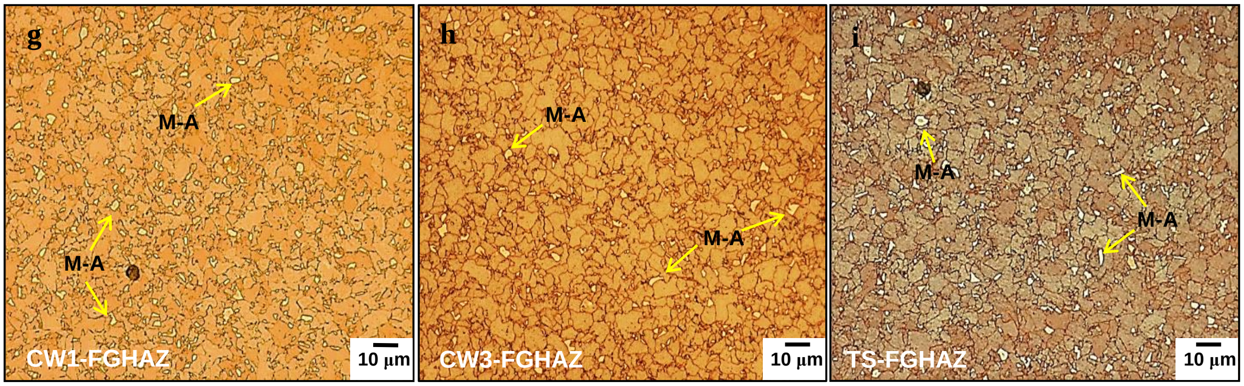

Fig. 6- Optical micrographs of the CGHAZ and FGHAZ for the CW1 sample (a,b,g), the CW3 sample (c,d,h) and the TS sample (e,f,i). Images (a-f) and (g-i) are from the CGHAZ and FGHAZ, respectively.

IV. DISCUSSION

The PAG size influences the phase transformation temperature and kinetics during cooling [40,41]. Ying-Qiao et al. [8] and Shome [42] reported that the size of PAGs in the HAZ depends on the local thermal cycle and the PAG size increases with increasing welding heat input. Refining the PAG size influences the transformation products, particularly the M-A constituents within the HAZ, which affect the toughness [11,12,32]. However, there has only been limited work done to correlate the PAG size and M-A constituents [11,12,32,43]. In addition, Bhadeshia [38,39], Yan et al. [44] and Matsuda et al. [45] have suggested that, in addition to the PAG size, cooling rate affects the morphology of the M-A constituents, which also affect the toughness of the welded steel. Kim et al. [46] have reported that M-A islands are the main metallurgical factor, which contribute to local embrittlement of microstructures of welded microalloyed steels. They also stated that the Charpy impact toughness of the CGHAZ of high strength low-carbon steels is a function of the fraction, morphology, carbon content and distribution of the M-A islands. The work done by Lan et al. [47] indicated that the relatively fast cooling rate in the HAZ of a low carbon steel led to the formation of slender M-A constituents with higher carbon levels and segregated silicon in the M-A islands, which resulted in an increase in the martensite hardness in the HAZ. As such, there is a concurrent effect of PAG size and cooling rate on the characteristics of the transformation products, in particular the M-A constituents, in the HAZ of microalloyed steel welds. Figure 6(a)-(i) depicts optical micrographs of the HAZ, revealing the PAGs and M-A constituents. The CGHAZ microstructure for the TS sample (with higher heat input) has large PAGs, polygonal ferrite (PF), granular bainite (GB), bainitic ferrite (BF) and a higher fraction of large M-A constituents, which are mostly formed along the PAG boundaries. In contrast with the TS sample, the CGHAZ microstructure of the CW1 sample is composed of finer PAGs, PF, GB and BF associated with fine, uniformly distributed M-A constituents. Due to the faster cooling rate in the CGHAZ of the CW3 sample (with the fastest cold wire addition and the lowest actual heat input) compared with the CW1 sample, smaller PAGs were formed in the CGHAZ of CW3, resulting in a lower fraction of elongated M-A constituents. However, longer M-A constituents are formed in the CGHAZ of the CW3 sample, which may be attributed to a greater reduction in the actual heat introduced to the weldment and the relatively fast cooling rate as a result of fast cold wire addition of 76.2 cm/min. However, the results indicate that the addition of the cold wire at 25.4 cm/min produced a favorable effect on the microstructure, which was beneficial to the toughness. The microstructure of the FGHAZ of the CW1 and CW3 samples is composed of PF and less GB and BF with smaller M-A constituents compared with that of the TS sample. However, fewer changes in the characteristics of the M-A constituents in the FGHAZ were observed by varying the cold wire addition. Phase fraction analysis of the transformation products in the CGHAZ and FGHAZ of the welded samples is indicated in Figure 7(b).

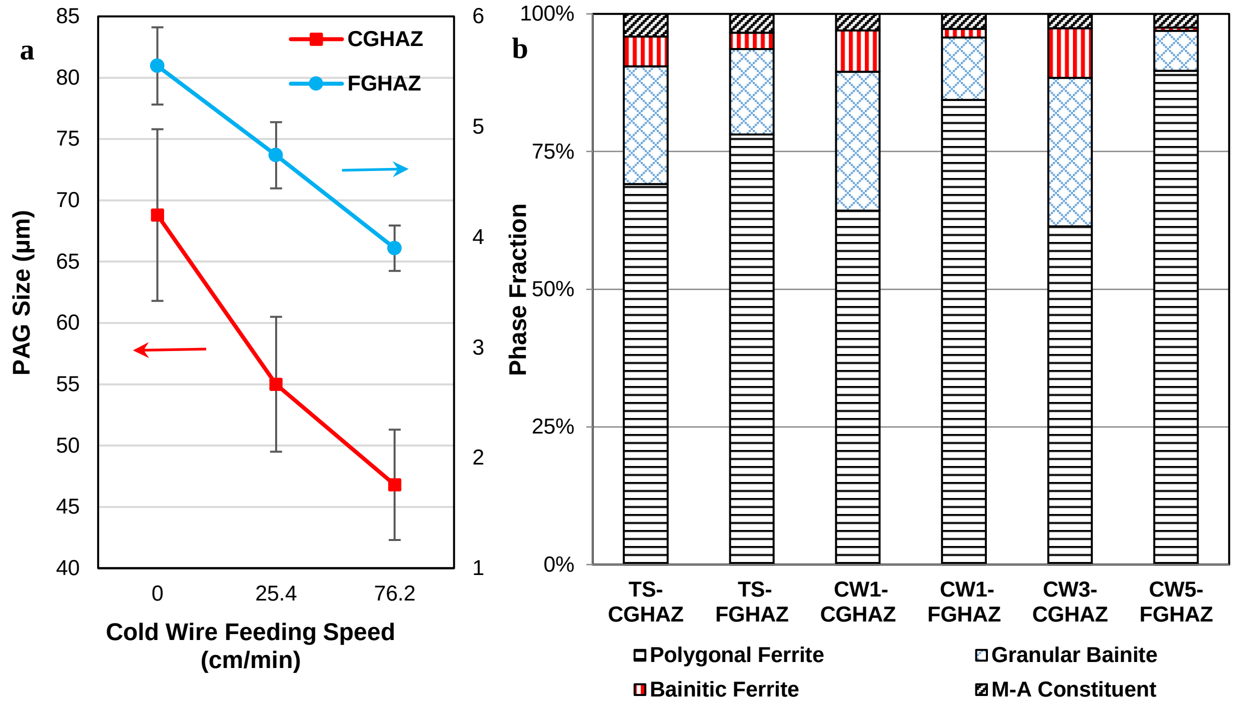

Fig. 7- (a) PAG size in the CGHAZ and FGHAZ and (b) microstructural constituent analysis in the FGHAZ and CGHAZ of microalloyed steel welds prepared by the CWTSAW (CW1 and CW3) and TSAW (TS) processes.

The M-A fraction in the CGHAZ, determined from the optical micrographs, was 4.1%, 3.0% and 2.7% for the TS, CW1 and CW3 samples, respectively, indicating a reduction in the fraction of M-A as a consequence of PAG size reduction [10,11] by cold wire addition. The M-A fractions in the CGHAZ of the TS, CW1 and CW3 samples, determined from the SEM micrographs, were 5.4%, 3.3% and 3.1%, respectively. These values are similar to those obtained using optical microscopy, which confirms the validity of M-A identification using optical images. The M-A fractions in the FGHAZ of the TS, CW1 and CW3 samples were 3.6%, 2.7% and 2.4%, respectively. Quantitative analysis of the M-A size distribution is shown in Figure 9. The sizes shown in Figure 9 are presented as an equivalent spherical diameter determined from the area of each microconstituent analyzed. As shown in Figure 6(b,d,f), the CGHAZ microstructure, particularly for the CW3 and TS samples, consists of more elongated shaped M-A constituents compared with the CW1 sample. A size distribution analysis was performed to evaluate the approximate size distribution of M-A constituents in the CGHAZ of the weld samples. In addition, image analysis carried out manually indicates that the fraction of M-A constituents in the CGHAZ with sizes larger than 1.5 µm for TS, CW1 and CW3 samples is 3.5%, 1.2% and 2.1%, respectively.

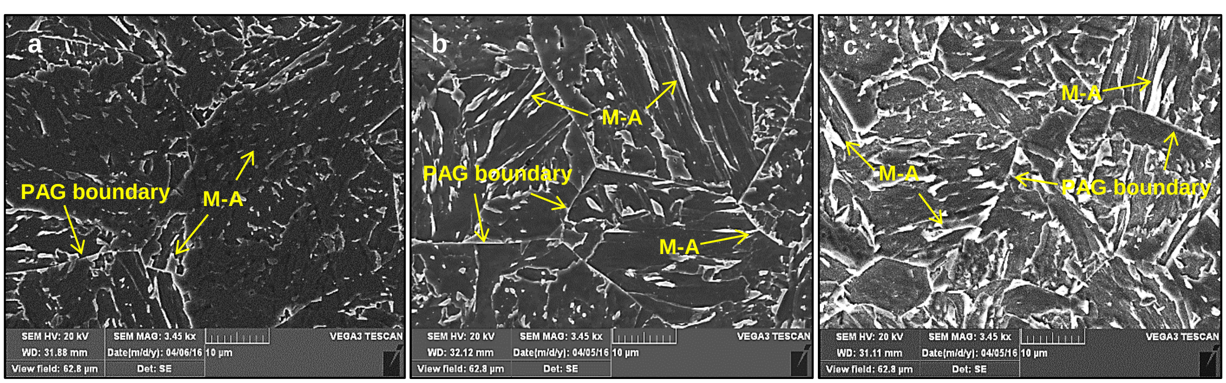

Fig. 8- SEM SE images of the CGHAZ for the (a) CW1, (b) CW3 and (c) TS samples.

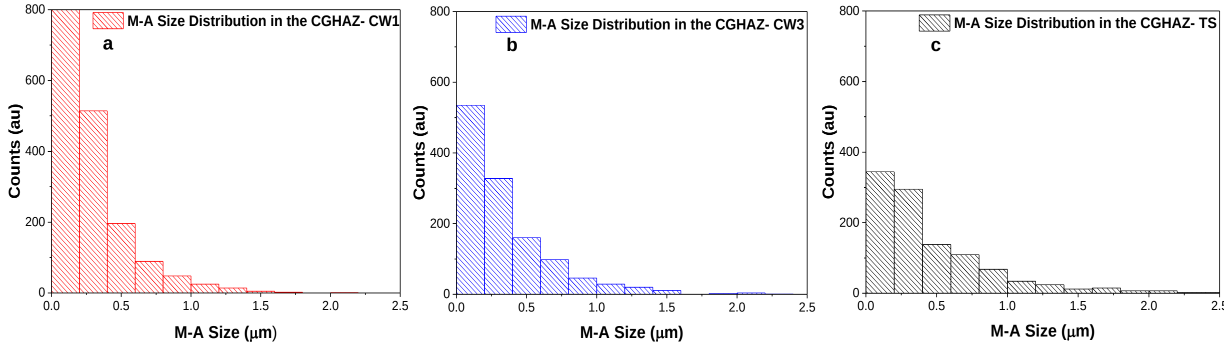

Fig. 9- Size distribution analysis of M-A constituent in the CGHAZ for the (a) CW1 (b) CW3 and (c) TS samples.

The fracture toughness of the CGHAZ of welded microalloyed steels is highly influenced by the shape, size, distribution and fraction of M-A constituents in the CGHAZ [10,11,46]. The distribution of M-A constituents in the CGHAZ of the weld samples was analyzed using the mean inter-particle spacing equation developed by Somekawa et al. [48]. The equation takes into account the relative volume fraction, mean particle size and mean inter-particle spacing.

$$\boldsymbol{\lambda_p} = \frac{\pi d_p^2}{2\sqrt{3} f_p} - \frac{\sqrt{2} d_p}{\sqrt{3}} \qquad [3]$$

where, λ_p, d_p and f_p are the mean inter-particle spacing, the mean particle size and the volume fraction, respectively. To calculate the inter-particle spacing of M-A constituents in the CGHAZ, the measured M-A constituent volume fraction along with the mean M-A sizes of 0.48 μm, 0.3 μm and 0.38 μm for the TS, CW1 and CW3 welds, respectively, were used. The calculated mean M-A constituent spacings in the CGHAZ of the TS, CW1 and CW3 welds were 4.9 μm, 2.5 μm and 4.5 μm, respectively. Figure 10(a,b) indicates the variation in the Charpy impact toughness in the HAZ as a function of M-A size and inter-particle spacing. As the M-A size and inter-particle spacing decrease in the CGHAZ of the CW1 sample, the fracture toughness increases. Accordingly, the formation of finely distributed M-A constituents in the CGHAZ of CW1 resulted in a beneficial effect on the fracture toughness.

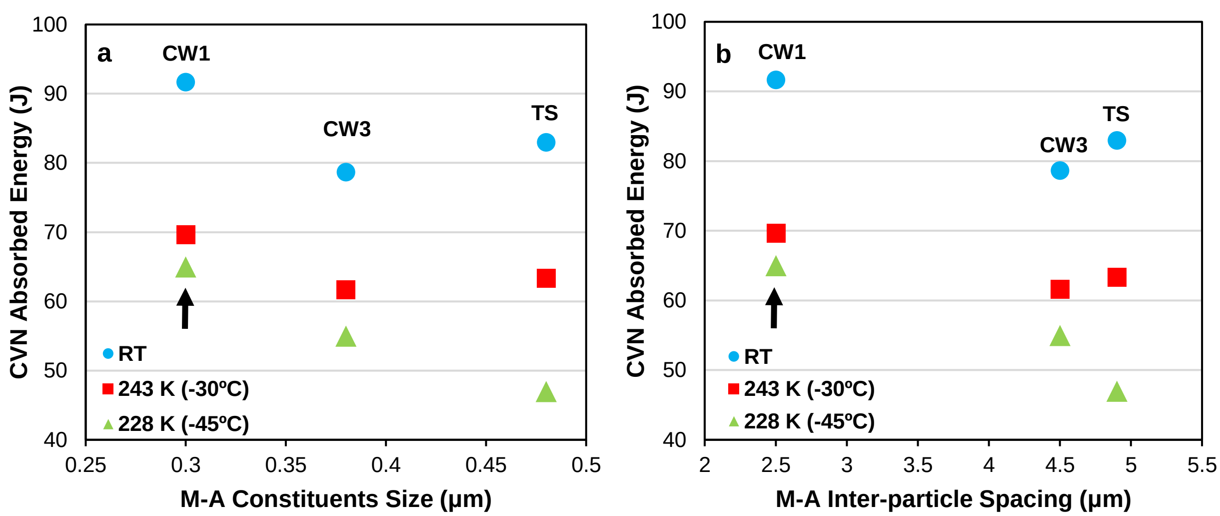

Fig. 10- Variation in the Charpy impact toughness as a function of (a) size and (b) inter-particle spacing of the M-A constituents in the CGHAZ of the CW1, CW3 and TS samples.

The larger M-A constituents in the CGHAZ of the TS sample are due to the higher martensite start temperature (Ms) for samples with larger PAGs [10,18,19,38]. Bhadeshia et al. [18,38], Heinze et al. [49] and Guimaraes [50] suggested that a decrease in Ms temperature corresponds to a decrease in the PAG size, which results in a lower volume fraction of martensite. According to the classical Koistinen-Marburger (KM) equation [51] and the geometrical partitioning model by Fisher et al. [52], the fraction of martensite is a function of the amount of undercooling below the Ms temperature. Based on the proposed model by Fisher et al. [52], the martensite volume fraction formed in the early stages of the transformation is proportional to the PAG size cubed; hence, "the fraction of the transformation needed to detect Ms is reached at a smaller undercooling when the PAG size is larger" [18]. Therefore, a coarser PAG size increases the fraction and size of the M-A constituent. Yu et al. [10] and Li et al. [11] showed that a coarse PAG size, associated with a coarse M-A constituent, is the dominant factor in promoting brittle fracture in the CGHAZ. Accordingly, there is a concurrent effect of both grain size refinement and M-A transformation, which plays a significant role in the strength and toughness of the HAZ. Due to the formation of the M-A constituent, there is a higher proportion of LBZs in the CGHAZ of the TS sample compared with the CW1 and CW3 samples. This shows up as higher microhardness values in the CGHAZ for the TS sample relative to the CWTSAW samples. Also, a narrower distribution of fine M-A constituents (LBZs) inside the ferritic matrix in the CGHAZ of the CW1 sample resulted in a higher fracture toughness for the HAZ at the various testing temperatures. However, coarser PAGs with large M-A constituents, which are mostly formed along the PAG boundaries, lead to inferior toughness properties in the HAZ of the TS sample. This inferior toughness, due to the formation of M-A constituents along PAG boundaries, has been confirmed by the research work done by Davis et al. [13,14] and Reichert et al. [15]. They found that the combination of an elongated shape and the formation of a network of M-A constituents along the PAG boundaries is most detrimental to fracture properties. With reference to the CW3 sample, Yan et al. [44] and Bhadeshia [38,39] have proposed that, in addition to the PAG size, the shape, size and distribution of the M-A constituents along with the martensite carbon content are influenced by the cooling rate in the HAZ, which affects toughness of welded microalloyed steels [53]. Elongated M-A constituents, with large inter-particle spacing, are formed in the CGHAZ of the CW3 sample due to the relatively faster cooling rate in the CGHAZ as a result of fast cold wire addition relative to the CW1 sample. This leads to a slight decrease in toughness for the HAZ of the CW3 sample compared with the CW1 sample (Figure 10). This phenomenon has also been confirmed by the work done by Davis et al. [13], Kim et al. [46] and Lan et al. [47], who have suggested that the morphology of martensite changes and the carbon content of martensite increases in the M-A constituents as the cooling rate in the CGHAZ increases. As such, the relatively faster cooling rate in the CGHAZ of the CW3 sample compared with the CW1 sample led to the formation of elongated M-A constituents with larger inter-particle spacing and higher carbon levels and segregated silicon to the M-A islands.

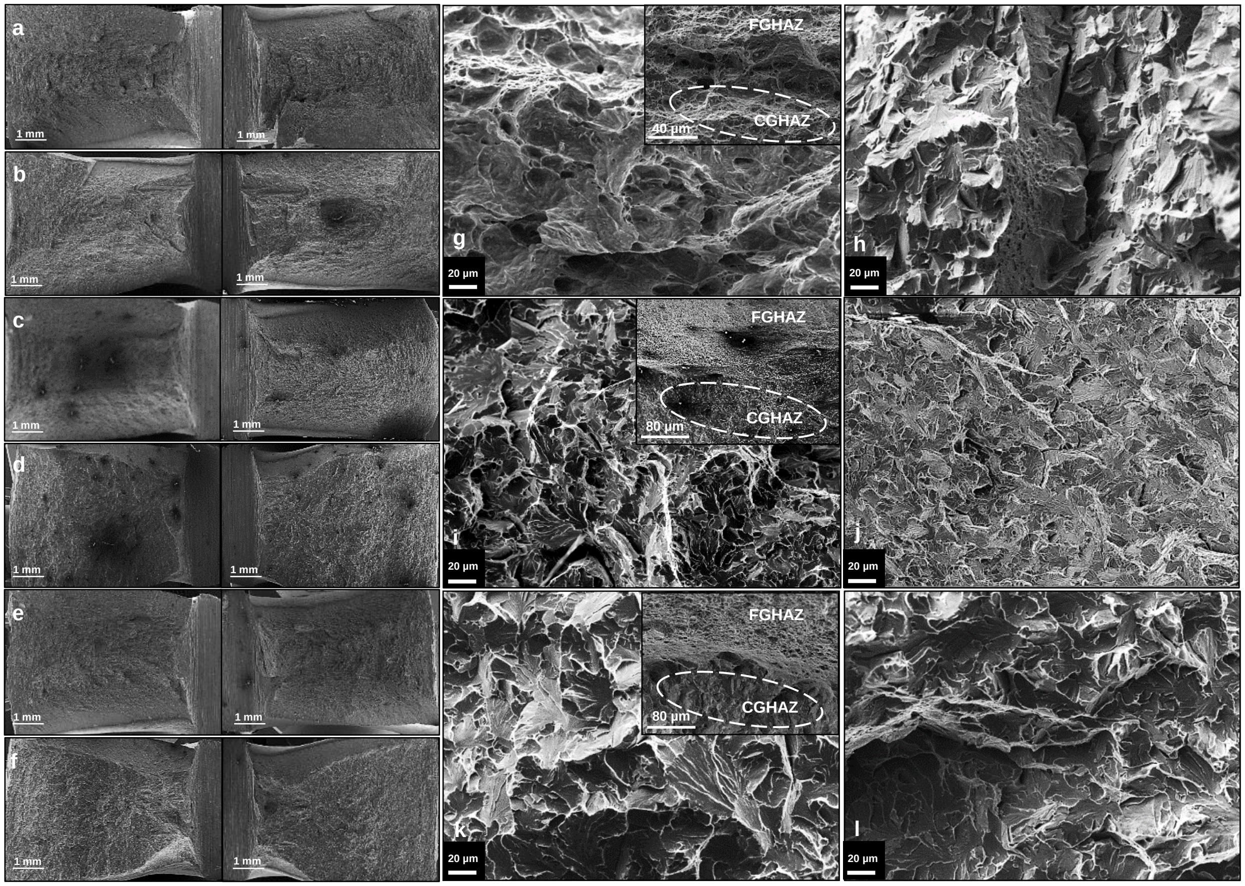

Fig. 11- SEM SE fractographs for the (a,b) CW1, (c,d) CW3 and (e,f) TS specimens. SEM SE micrographs showing the fracture surfaces in the CGHAZ for the (g,h) CW1, (i,j) CW3 and (k,l) TS specimens. The insets in (g), (i) and (k) show the boundary between the FGHAZ and CGHAZ in the weld specimens. Micrographs (a,c,e,g,i,k) and (b,d,f,h,j,l) are from Charpy samples tested at RT and 243 K (-30°C), respectively.

According to the impact toughness results shown in Figure 10, the toughness of the HAZ of the TS sample was lower compared with that of the CW1 sample, which is attributed to the formation of a high fraction of elongated and widely spaced M-A constituents inside and along the PAG boundaries as a result of the higher actual heat input. Lowering the actual heat introduced to the weldment, by addition of the cold wire at 25.4 cm/min, altered the size, shape, distribution and fraction of the M-A constituent, leading to an improvement in the HAZ toughness of the CW1 sample. The reduction in toughness by increasing welding heat input has been confirmed in the literature [16,42,54]. However, when the cold wire was fed at a faster rate of 76.2 cm/min, the HAZ toughness was diminished due to the formation of large, widely spaced elongated M-A constituents inside and along PAG boundaries as a result of the faster cooling rate. The influence of the fast cooling rate on the fracture toughness of the HAZ of microalloyed steels has been well documented previously through the work done by Hutchinson et al. [55], Yan et al. [44] and Bhadeshia [38,39]. A faster cooling rate provides a greater driving force for martensite transformation, which increases the fraction of martensite within the M-A constituents in the CGHAZ [47]. The faster cooling rate also influences the morphology of the M-A constituents, leading to more elongated shapes and detrimental effects on fracture toughness [38,44,55]. Cracks, initiated at large elongated M-A constituents, can connect and form a long continuous long crack, resulting in brittle cleavage fracture. A low fraction of finely distributed fine M-A constituents can act as crack arrestors for secondary cracks, which is beneficial to toughness [56]. In addition, it is generally accepted that the formation of large slender shaped M-A constituents in the CGHAZ of welded microalloyed steels is detrimental to the HAZ fracture toughness. However, regardless of the shape and size of M-A constituents, spacing of the hard phases in the soft matrix (i.e., ferritic matrix in the CGHAZ of the welded microalloyed steel) influences the propagation of the cracks in a manner similar to composite materials. As the spacing between hard particles (or phases) decreases, the crack will face a hard phase at a shorter distance, which stops the crack or makes it harder for the crack to propagate. In addition, slender shaped hard phases (or particles) promote the propagation of any cracks due to the higher stress concentration at the tip of the sharp particles.

The fracture surface morphologies of the HAZ at RT and 243 K (-30ºC) for the CW1, CW3 and TS Charpy samples are illustrated in Figure 11(a,b,g,h), 11(c,d,i,j) and 11(e,f,k,l), respectively. The boundary between the CGHAZ and FGHAZ on the fracture surface is shown in the inset micrographs in Figure 11(g,i,k). The fracture surface for the FGHAZ and CGHAZ of the CW1 weld sample at RT is fully ductile and the fracture mechanism involves microvoid coalescence (MVC). However, the fracture mechanism in the FGHAZ and CGHAZ for both the CW3 and TS samples at RT is different, i.e., MVC and quasi-cleavage, respectively, resulting in ductile and quasi-brittle fracture in the FGHAZ and CGHAZ at RT. Due to the large PAG size in the CGHAZ of the TS sample, large cleavage facets are present on the fracture surface. Moreover, the formation of large, elongated and widely spaced M-A constituents in the CGHAZ of the CW3 and TS samples contributed to lowering of the Charpy energy in the HAZ. A combination of MVC and quasi-cleavage fracture is seen on the CGHAZ fracture surface of the CW1 sample tested at 243 K (-30°C). However, the CGHAZ fracture surface of the TS sample consists of a mixture of cleavage and intergranular facets, resulting in brittle fracture in the CGHAZ of the TS sample tested at 243 K (-30°C) [57]. Similar to the TS sample, intergranular fracture along with cleavage is the dominant fracture mechanism of the CGHAZ of the CW3 sample, due to the formation of the elongated M-A constituents along the PAGs with large inter-particle spacing. Finer cleavage facets are evident on the CGHAZ fracture surface of the CW3 sample because of the formation of a finer PAG size in the CGHAZ of the CW3 sample due to the faster cooling rate (lower actual heat input by faster cold wire addition) in the CGHAZ compared with the other two weld samples.

The fracture mechanism at 228 K (-45ºC) in the FGHAZ of the three weld samples was MVC, however, cleavage and intergranular fracture were observed to be the dominant mechanism in the CGHAZ of the weld samples. Since, the fracture mechanism of the three weld samples at 228 K (-45ºC) was similar to the fracture mechanism for the CW3 and TS samples at 243 K (-30°C), the fractographs at 228 K (-45ºC) are not shown here. The M-A constituent is significantly harder than the internal grain microstructure, so that cracks initiate easily along large M-A constituents. Aucott et al. [58] have suggested that the toughness of a welded X65 linepipe steel was reduced by formation of coarse size particles with large inter-particle spacing. Moeinifar et al. [1] concluded from their microstructural study on multiple-wire TSAW samples that the size and shape of M-A constituents are significant factors affecting the Charpy impact properties of the CGHAZ and that microcrack nucleation may occur from M-A islands at the intersection of PAG boundaries. Moreover, Li et al. [56] found that an intercritically reheated CGHAZ demonstrated the lowest toughness, due to the presence of M-A constituents with high carbon content martensite. The large elongated shaped M-A constituents with large inter-particle spacing in the CGHAZ of the CW3 and TS samples of this work formed mostly along the PAG boundaries and can promote the formation of microcracks, resulting in brittle/quasi-brittle fracture in the HAZ.

V. CONCLUSIONS

The influence of the cold wire addition rate, in the recently developed cold wire tandem submerged arc welding (CWTSAW) process, on the microstructural characteristics and mechanical properties of the HAZ of a welded microalloyed steel has been studied for the first time. Cold wire addition resulted in a reduction in the prior austenite grain (PAG) size in the coarse grained heat affected zone (CGHAZ). Microstructural analysis indicated that the fraction of martensite-austenite (M-A) constituents in the CGHAZ was reduced and the distribution, size and shape were altered, when a cold wire was added to the TSAW process. The cold wire addition at 25.4 cm/min showed a reduction in the fraction of M-A constituents along with a uniform distribution of finer M-A constituents in the ferritic matrix due to a reduction in the actual welding heat input and the PAG size, which resulted in an improvement in fracture toughness of the HAZ. The changes to the fraction and characteristics of the M-A constituents in the HAZ of the cold wire sample (25.4 cm/min) relative to the sample with no cold wire are attributed to the lower actual heat introduced to the weldment and the resulting faster cooling rate, lower peak temperature and the formation of finer PAGs by cold wire addition. Although the PAG size was further reduced when the cold wire was fed at 76.2 cm/min (compared with the cold wire (25.4 cm/min) and TSAW weld samples), due to a faster cooling rate in the CGHAZ of the 76.2 cm/min cold wire sample, elongated shaped M-A constituents were formed. The relatively large elongated M-A constituents with large inter-particle spacing, which mostly formed along the PAG boundaries in the CGHAZ, of the TSAW and cold wire (76.2 cm/min) samples compared with those of the cold wire sample (25.4 cm/min) led to inferior toughness properties in the HAZ of the former samples, since the larger M-A constituents can stimulate the formation of microcracks leading to intergranular fracture.

ACKNOWLEDGMENTS

The authors would like to thank the Natural Sciences and Engineering Research Council (NSERC) of Canada, Evraz Inc. NA, TransCanada PipeLines Ltd., Enbridge Pipelines Inc., UT quality Inc. and Alliance Pipeline Ltd for financial support. Special thanks go to the Research and Development Division of Evraz Inc. NA for providing equipment and technical assistance to conduct the welding runs and Charpy testing.

REFERENCES

[1] S. Moeinifar, A. H. Kokabi, and H. R Madaah Hosseini: *J. Mater. Process. Technol.*, 2011, vol. 211, pp. 368–75.
[2] D. V. Kiran, S.A. Alam, and A. De: *J. Mater. Eng. Perform.*, 2013, vol. 22, pp. 988–94.
[3] ESAB: *Submerged Arc Welding (Technical Handbook)*, TX, 2013.
[4] D.M. Viano, N.U. Ahmed, G.O. Schumann, D.M. Viano, N.U. Ahmed, and G.O. Schumann: *Sci. Technol. Weld. Join.*, 2000, vol. 5, pp. 26–34.
[5] Y. Watanabe, K. Yoshii, and Y. Yoshida: *Development of 590N/mm2 Steel with Good Weldability for Building Structures, Technichal Report No. 90*, 2004.
[6] D.W. Nugent, R.M., Dybas, R.J., Hunt, J.F., Meyer: *Submerged Arc Welding. AWS Welding Handbook*, 8th Ed., American Welding Society, Miami, 2009.
[7] S. Shen, I.N.A. Oguocha, and S. Yannacopoulos: *J. Mater. Process. Technol.*, 2012, vol. 212, pp. 286–94.
[8] Ying Qiao Zhang, Han Qian Zhang, Jin Fu Li, and Wei Ming Liu: *J. Iron Steel Res. Int.*, 2009, vol. 16, pp. 73–80.
[9] Z.H. Xia, X.L. Wan, X.L. Tao, and K.M. Wu: *Adv. Mater. Res.*, 2012, vol. 538–541, pp. 2003–8.
[10] L. Yu, H.H. Wang, T.P. Hou, X.L. Wang, X.L. Wan, and K.M. Wu: *Sci. Technol. Weld. Join.*, 2014, vol. 19, pp. 708–14.
[11] X. Li, X. Ma, S.V. Subramanian, Ch. Shang, and R.D.K. Misra: *Mater. Sci. Eng. A*, 2014, vol. 616, pp. 141–47.
[12] X. Li, Y. Fan, X. Ma, S.V. Subramanian, and Ch. Shang: *Mater. Des.*, 2015, vol. 67, pp. 457–63.
[13] C.L. Davis and J.E. King: *Mater. Sci. Technol.*, 1993, vol. 9, pp. 8–15.
[14] C.L. Davis and J.E. King: *Metall. Mater. Trans. A*, 1994, vol. 25, pp. 563–73.
[15] J.M. Reichert, T. Garcin, M. Militzer, and W.J. Poole: in *9th Int. Pipeline Conf.*, American Society of Mechanical Engineering, Calgary, AB, 2014.
[16] S. Moeinifar, A.H. Kokabi, and H.R. Madaah Hosseini: *Mater. Des.*, 2010, vol. 31, pp. 2948–55.
[17] E. Gharibshahiyan, A. Honarbakhsh, N. Parvin, and M. Rahimian: *Mater. Des.*, 2011, vol. 32, pp. 2042–48.
[18] H.S. Yang and H.K.D.H. Bhadeshia: *Scr. Mater.*, 2009, vol. 60, pp. 493–95.
[19] A. Garcia-Junceda, C. Capdevila, F.G. Caballero, C. Garcia, and D. Andre: *Scr. Mater.*, 2008, vol. 58, pp. 134–37.
[20] M.F. Mruczek and P.J. Konkol: *Cold Wire Feed Submerged Arc Welding: Technical Report*, Advanced Technology Institute (ATI), Johnstown, PA, 2006.
[21] M. Ramakrishnan and V. Muthupandi: *Int. J. Adv. Manuf. Technol.*, 2012, pp. 1–12.
[22] M. Ramakrishnan, K. Padmanaban, and V. Muthupandi: *Int. J. Adv. Manuf. Technol.*, 2013, vol. 68, pp. 293–316.
[23] M. Mohammadijoo, S. Kenny, J.B. Wiskel, D.G. Ivey, and H. Henein: in *54th Anuual Conf. Metall.*, Canadian Institute of Mining, Metallurgy and Petroleum, Toronto, ON, 2015, pp. 1–13.
[24] M. Mohammadijoo, S. Kenny, L. Collins, H. Henein, and D.G. Ivey: *Int. J. Adv. Manuf. Technol.*, 2016, doi: 10.1007/s00170-016-8910-z, pp. 1–15.
[25] N. Shikanai, S. Mitao, and S. Endo: *Recent Development in Microstructural Control Technologies through the Thermo-Mechanical Control Process (TMCP) with JFE Steel's High-Performance: JFE Technical Report No. 18 Plates*, JFE Steel, Tokyo, 2007.
[26] K.E. Easterling: *Introduction to the Physical Metallurgy of Welding*, Butterworth-Heinemann Ltd, Oxford, 1992.
[27] B. De Meester: *ISIJ Int.*, 1997, vol. 37, pp. 537–51.
[28] L.P. Connor and R.L. O'Brien: *Welding Handbook: Welding Technology*, American Welding Society, Miami, 1987.

[29] ASTM: *ASTM E23-12C: Standard Test Methods for Notched Bar Impact Testing of Metallic Materials*, ASTM International, PA, 2012.
[30] ASTM: *E384: Standard Test Method for Knoop and Vickers Hardness of Materials*, ASTM International, PA, 2012.
[31] ASTM: *E3-11: Standard Guide for Preparation of Metallographic Specimens*, ASTM International, PA, 2011.
[32] Y. Prawoto, N. Jasmawati, and K. Sumeru: *J. Mater. Sci. Technol.*, 2012, vol. 28, pp. 461–66.
[33] ASTM: *E112-12: Standard Test Methods for Determining Average Grain Size*, ASTM International, PA, 2012.
[34] F.S. LePera: *Metallography*, 1979, vol. 12, pp. 263–68.
[35] M. Mohammadijoo, H. Henein, and D.G. Ivey: in *Microsc. Soc. Canada 43rd Annu. Meet.*, Edmonton, AB, 2016, pp. 68–69.
[36] ASTM: *ASTM E562-11: Standard Test Method for Determining Volume Fraction by Systematic Manual Point Count*, ASTM International, PA, 2011.
[37] S.M. Graham: *J. Test. Eval.*, 2005, vol. 33.
[38] H.K.D.H. Bhadeshia: in *Int. Semin. Weld. High Strength Pipeline Steels*, CBMM and The Minerals, Metals and Materials Society, The Minerals, Metals and Materials Society (TMS), USA, 2013, pp. 99–106.
[39] H.K.D.H. Bhadeshia: *Mater. Sci. Forum*, 2014, vol. 783–786, pp. 2129–35.
[40] M. Shome, O.P. Gupta, and O.N. Mohanty: *Metall. Mater. Trans. A*, 2004, vol. 35A, pp. 985–96.
[41] G. Spanos, R.W. Fonda, R.A. Vandermeer, and A. Matuszeski: *Metall. Mater. Trans. A*, 1995, vol. 26A, pp. 3277–93.
[42] M. Shome: *Mater. Sci. Eng. A*, 2007, vol. 445–446, pp. 454–60.
[43] R. Cao, J. Li, D.S. Liu, J.Y. Ma, and J.H. Chen: *Metall. Mater. Trans. A*, 2015, vol. 46A, pp. 2999–3014.
[44] P. Yan and H.K.D.H. Bhadeshia: *Mater. Sci. Technol.*, 2015, vol. 31, pp. 1066–76.
[45] F. Matsuda, K. Ikeuchi, Y. Fukada, Y. Horii, H. Okada, T. Shiwaku, C. Shiga, and S. Suzuki: *Transcations JWRI*, 1995, vol. 24, pp. 1–24.
[46] B.C. Kim, S. Lee, N.J. Kim, and D.Y. Lee: *Metall. Mater. Trans. A*, 1991, vol. 22, pp. 139–49.
[47] L. Lan, Ch. Qiu, and D. Zhao: *J. Mater. Sci.*, 2012, vol. 47, pp. 4732–42.
[48] H. Somekawa and T. Mukai: *Mater. Trans.*, 2006, vol. 47, pp. 995–98.
[49] C. Heinze, A. Pittner, M. Rethmeier, and S.S. Babu: *Comput. Mater. Sci.*, 2013, vol. 69, pp. 251–60.
[50] J.R.C. Guimaraes and P.R. Rios: *J. Mater. Sci.*, 2010, vol. 45, pp. 1074–77.
[51] D.P. Koistinen and R.E. Marburger: *Acta Metall.*, 1959, vol. 7, pp. 59–60.
[52] J.C. Fisher, J.H. Hollomon, and D. Turnbull: *Trans. Am. Inst. Min. Metall. Eng.*, 1949, vol. 185, pp. 691–700.
[53] C.R. Brooks: *Principles of the Heat Treatment of Plain Carbon and Low-Alloy Steel*, ASM International, Ohio, 1996.
[54] G.-L. Liang, S.-W. Yang, and H.-B. Wu: *Rare Met.*, 2013, vol. 32, pp. 129–33.
[55] B. Hutchinson, J. Komenda, G.S. Rohrer, and H. Beladi: *Acta Mater.*, 2015, vol. 97, pp. 380–91.
[56] Y. Li and T.N. Baker: *Mater. Sci. Technol.*, 2010, vol. 26, pp. 1029–40.
[57] M. Shome, O.P. Gupta, and O.N. Mohanty: *Metall. Mater. Trans. A*, 2004, vol. 35A, pp. 985–96.
[58] L. Aucott, S.W. Wen, and H. Dong: *Mater. Sci. Eng. A*, 2015, vol. 622, pp. 194–203.

Figure Captions:

Fig. 1- CWTSAW process setup. (a) Schematic view of joint configuration along with the positioning of the electrodes and cold wire and (b) welding setup designed at Evraz Inc. NA.

Fig. 2- (a) Schematic view of the CVN specimen extraction from the weld sample. (b) Microhardness mapping along the BM, HAZ and WM of a typical weld prepared by CWTSAW. The micrograph in the inset shows an indentation in the CGHAZ.

Fig. 3- Charpy impact toughness of the HAZ for steel samples welded by TSAW (no cold wire) and CWTSAW (cold wire addition at 25.4 cm/min and 76.2 cm/min). (a), (b) and (c) represent Charpy results at room temperature (RT), 243 K (-30ºC) and 228 K (-45ºC), respectively.

Fig. 4- Macrographs of welded samples: (a) TS, (b) CW1 and (c) CW3.

Fig. 5- (a) Microhardness variation within the weld samples. (b) Average microhardness, with the standard deviation, for the FGHAZ and CGHAZ of steel samples welded by the CWTSAW (cold wire addition at 25.4 cm/min and 76.2 cm/min) and TSAW (no cold wire).

Fig. 6- Optical micrographs of the CGHAZ and FGHAZ for the CW1 sample (a,b,g), the CW3 sample (c,d,h) and the TS sample (e,f,i). Images (a-f) and (g-i) are from the CGHAZ and FGHAZ, respectively.

Fig. 7- (a) PAG size in the CGHAZ and FGHAZ and (b) microstructural constituent analysis in the FGHAZ and CGHAZ for microalloyed steels welded by the CWTSAW (CW1 and CW3) and TSAW (TS) processes.

Fig. 8- SEM SE images of the CGHAZ for the (a) CW1, (b) CW3 and (c) TS samples.

Fig. 9- Size distribution analysis of M-A constituent in the CGHAZ for the (a) CW1 (b) CW3 and (c) TS samples.

Fig. 10- Variation in the Charpy impact toughness as a function of (a) size and (b) inter-particle spacing of the M-A constituents in the CGHAZ of the CW1, CW3 and TS samples.

Fig. 11- SEM SE fractographs for the (a,b) CW1, (c,d) CW3 and (e,f) TS specimens. SEM SE micrographs showing the fracture surfaces in the CGHAZ for the (g,h) CW1, (i,j) CW3 and (k,l) TS specimens. The insets in (g), (i) and (k) show the boundary between the FGHAZ and CGHAZ in the weld specimens. Micrographs (a,c,e,g,i,k) and (b,d,f,h,j,l) are from Charpy samples tested at RT and 243 K (-30°C), respectively.

Tables:

Table I. X70 microalloyed steel and electrode compositions (wt%)

X70 composition								
C	P	S	Mn	Si	N	V+Mo+Nb+Ti	Cu+Ni+Cr+Sn+Al+Ca	Pcm
0.04	0.01	0.001	1.76	0.24	0.0098	0.21	0.60	0.175

Electrode and cold-wire composition									
Symbol	C	P	S	Mn	Si	Mo	Ni	Cr	Cu
BA-S2Mo	0.10	0.007	0.01	1.04	0.1	0.56	0.02	0.03	0.03

Table II. Welding process parameters

Process Parameter	**Unit**	**Value**		
Current- Lead Electrode	A	1040		
Current- Trail Electrode	A	830		
Voltage- Lead Electrode	V	30		
Voltage- Trail Electrode	V	34		
Feed Speed- Lead Electrode	cm/min (in/min)	254 (100)		
Feed Speed- Trail Electrode	cm/min (in/min)	203 (80)		
Welding Travel Speed	cm/min (in/min)	160 (63)		
		CW1	**CW3**	**TS**
Cold Wire Position	--	Lagging	Lagging	NA
Cold Wire Angle	degree	63	63	NA
Cold Wire Feed Speed	cm/min (in/min)	25.4 (10)	76.2 (30)	NA